Peer-reviewed version available at *Atmosphere* **2018**, *9*, 487; doi:10.3390/atmos9120487

Improving Seasonal Prediction of East Asian Summer Rainfall: Experiments with NESM3.0

Young-Min Yang[1,2], Bin Wang [*1,2], Juan Li [1]

1 Key Laboratory of Meteorological Disaster of Ministry of Education and Earth System Modeling Center, Nanjing University of Information Science and Technology, Nanjing, China

2 Department of Atmospheric Sciences and International Pacific Research Center, University of Hawaii, Honolulu, Hawaii 96822, USA

*Corresponding Author: Dr. Bin Wang, email address: wangbin@hawaii.edu

Abstract

It has been an outstanding challenge for global climate models to simulate and predict East Asia (EA) summer monsoon (EASM) rainfall. This study evaluates the dynamical hindcast skills with the newly developed Nanjing University of Information Science and Technology Earth System Model version 3.0 (NESM3.0). To improve the poor prediction of an earlier version of NESM3.0, we have modified convective parameterization schemes to suppress excessive deep convection and enhance insufficient shallow and stratiform clouds. The new version of NESM3.0 with modified parameterizations (MOD hereafter) yields significantly improved rainfall prediction in the northern and southern China but not over the Yangtze River Valley. The improved prediction is primarily attributed to the improvements in the predicted climatological summer mean rainfall and circulations, seasonal march of the subtropical rain belt, Nino 3.4 SST anomaly, and the rainfall anomalies associated with the development and decay of El Nino events. However, the MOD still has notable biases in the predicted leading mode of interannual variability of precipitation. The leading mode captures the dry (wet) anomalies over the South China Sea (northern EA) but misplaced precipitation anomalies over the Yangtze River Valley. The model can capture the interannual variation of the circulation

indices very well, but the bias in the circulation-rainfall connection caused predicted rainfall errors. The results here suggest that over EA land regions, the skillful rainfall prediction relies on not only model's capability in predicting better summer mean and seasonal march of rainfall and ENSO teleconnection with EASM, but also accurate prediction of the leading modes of interannual variability.

Key words: East Asian summer monsoon, Seasonal prediction, dynamic prediction, summer rainfall prediction, NESM3.0, ENSO teleconnection

1. Introduction

Seasonal prediction of the land monsoon precipitation has been an outstanding challenge since 1886 when Indian monsoon rainfall prediction started (Webster 2006). Over the East Asia (EA) and western North Pacific (WNP) region, the atmospheric general circulation models have notorious problems in simulation of the climatological monsoon trough and subtropical high as well as the subtropical frontal rain belt (Kang et al. 2002). A particular challenge is that the vigorous monsoon-ocean interaction must be considered in the dynamic simulation and prediction of monsoon precipitation (Wang et al. 2004, 2005).

Seasonal predictions using coupled climate models have been progressively improved by continuous efforts to improve initializations, model physical parameterizations and horizontal and vertical resolutions (Yang et al. 2008; Tompkins et al. 2017). Previous studies have shown considerable prediction skills for prediction of the EASM index. However, prediction of summer precipitation using coupled climate models remains at a very low-level of skills, particularly over the EA land region. Striking deficiencies are observed over the South China Sea and WNP region, where considerable model biases exist in both the amplitude and phase of the annual cycle; in addition, its interannual variability is underestimated (Lee et al. 2010).

To improve rainfall prediction over EA, multi-model ensemble (MME) predictions have been conducted (Wang et al 2009, Lee et al. 2015). Based on evaluation of the MME seasonal hindcasts performed by 14 climate models that participate in the Climate Prediction and its Application to Society (CliPAS) project and 6 models from the DEMETER project, Wang et al. (2009) concluded that forecast of monsoon precipitation remains a major challenge and the seasonal rainfall predictions over land and during local summer have little skill. Lee et al (2015)

added downscaling methods to CilPAS prediction data in order to enhance prediction skill but there is no considerable improvement.

Recently, the third version of the Nanjing University of Information Science and Technology (NUIST) Earth System Model (NESM3.0 for short hereafter) has been developed to provide a numerical model for earth system studies, to project future climate changes and to simulate past climate changes, as well to conduct subseasonal-to-seasonal prediction. A historical experiment of the NESM3.0 based on coupled model intercomparison project phase (CMIP) 6 protocol was conducted. The results showed that the NESM3.0 generally well reproduces the mean state of rainfall, EASM onset date, the leading mode of interannual variability, monsoon-ENSO relationship during mature phase and western Pacific subtropical high (WPSH)-EA rainfall teleconnection over EA.

This study documents the seasonal prediction skills of the NESM3.0 over EA and elaborates and discusses how the significant prediction kill was achieved and what are the possible causes for the deficiencies. Section 2 introduces the NESM3.0 and presents data and initialization methods. In section 3, we discuss how the prediction skill for EASM is improved based on the diagnostic analysis of the

temporal and spatial structures of the large-scale dynamic systems. The last section presents a summary.

2. Model, data and initialization

2.1. The NESM3.0 Model

The newly developed NESM3.0 is a fully coupled climate system and earth system model. The ocean component of the NESM3.0 is Ocean PArallelise (OPA), which is the ocean part of the Nucleus for European Modelling of the Ocean (NEMO) v3.4. The sea ice model in the NESM3.0 is CICE v4.1, which is originally developed at the Los Alamos National Laboratory. The atmosphere and land components of the NESM v3.0 are the ECHAM v6.3 atmospheric model and the associated land surface model—the Jena Scheme for Atmosphere Biosphere Coupling in Hamburg (JSBACH). The four model components are coupled through the Ocean-Atmosphere-Sea-Ice-Soil Model Coupling Toolkit version 3.0 (OASIS3-MCT_3.0), which is a fully parallelized tool to synchronize, interpolate and exchange the coupling fields among the atmospheric, oceanic and sea ice component models. The resolution of the atmospheric model is T63 horizontally (about 200 km) and 47 levels vertically with 0.01 hPa as the model top. The land surface model has the same horizontal resolution as the atmospheric model. The ocean model has a resolution

of 1°latitude and longitude grid with the meridional resolution being refined to 1/3° over the equatorial region, and it has 46 vertical layers with the first 15 layers at the top 100 meters. The sea ice model resolution is about 1° latitude by longitude with four sea ice layers and one snow layer on the top of the ice surface. The details of the NESM3.0 is referred to Cao et al. (2018) and Yang and Wang (2018).

The ECHAM v6.3 and JSBACH model are originally developed at the Max Planck Institute (Stevens et al. 2017). The convective parameterization is based on the mass-flux framework developed by Tiedtke (1989) and further modified by Nordeng (1994) (TDK, hereafter). The stratiform cloud scheme contains prognostic equations for the vapor, liquid, and ice phase of water, a cloud microphysical scheme, and a diagnostic cloud cover scheme. The JSBASH land surface model simulates the fluxes of energy, momentum, moisture, and tracer gases between the land surface and the atmosphere.

2.2 Major improvement of the early version of the model

The early developmental version of NESM3.0 reproduces reasonably well global energy balance, climatology and major modes of climate variability but it has biases in the climatology over EA and WNP. The model overproduces heavy rain belts over the tropical monsoon trough extending from India to the Philippine Sea.

The model also underproduces major subtropical rainfall over China, Japan and Korea. The northward flow over the eastern China shifted westward and was weaker than the observation. Observed studies revealed that shallow (20-30%) and stratiform (60-80%) clouds occur frequently than deep cloud (20-30%) during summer season (Wen et al. 2016) and the contribution of stratiform rainfall to total precipitation amount is about 40-50% (Yang and Smith, 2008). However, over EA and WNP convective precipitation accounts for over 90% of the total precipitation in the model. This suggests that the excessive precipitation in the model may be mainly attributed to excessive deep convection, particularly in summer; hence it is critical to suppress deep convection and enhance shallow and stratiform clouds for improvement of simulated rainfall over EA.

Given the problems of the early version, we need to improve the model's capacity in simulating realistic EA-WNP summer monsoon while keeping global energy and water balance unaffected. For this purpose, we implemented four modified parameterizations to the NESM3.0. First, a boundary layer depth-dependent convective inhibition (INH) was added to the convective scheme to suppress deep convection (Yang and Wang 2018). The INH suppresses deep clouds when the boundary layer depth is relatively shallow, which can reduce the precipitation over the SCS and Philippine Sea where the earlier NESM3.0

overestimates precipitation. Second, we added a bottom-heavy diffusivity in the shallow convection scheme (SHC) (Yang and Wang 2018). In the earlier version of the NESM3.0, it is found that vertical mixing between the lower troposphere and the top of BL is insufficient. The modified shallow convective scheme is effective to enhance shallow convection in the lower troposphere. Third, we changed the conversion rate from convective cloud water to rain. This changes increased moisture supply to stratiform clouds meanwhile reduced the amount of convective precipitation. When the conversion rate decreases, less convective cloud water converts to rainfall and thus convective precipitation decreases. The remaining cloud water in the updraft is detrained to the ambient air, which leads to enhanced stratiform cloud. Fourth, the entrainment rates in deep and shallow clouds have been adjusted. An increasing entrainment rate tends to suppress deep convection. When the convective plume rises up, a large entrainment rate decreases the buoyancy of updraft quickly by enhancing mixing with relatively dry and cold environmental air; th…us cloud development tends to be suppressed. In addition, we tuned cloud cover scheme and cloud microphysics to reduce biases in global energy balance (e.g. SST, short/long wave radiation at the top of Atmosphere). Note that the modified parameterizations do not appreciably change global precipitation climatology and internal modes (e.g., ENSO simulations).

Peer-reviewed version available at Atmosphere 2018, 9, 487; doi:10.3390/atmos9120487

For clarity, the prediction with the earlier version of the model (without the modified parameterizations) is called the 'CTL' and the prediction using the model with the modified parameterizations is called the 'MOD'. A parallel suits of 30-year hindcast experiments was carried out in order to identify and understand the impacts of the model modifications.

2.3 The data and initialization

The National Centers for Environmental Prediction-Department of Energy (NCEP-DOE) Reanalysis II data (Kanamitsu et al. 2002) are used to represent observed winds and geopotential heights. The observed precipitation data are derived from the Global Precipitation Climatology Project (GPCP) daily data (Adler et al. 2003). For monthly mean sea surface temperature (SST), we used the National Oceanic and Atmospheric Administration Extended Reconstructed SST (ERSST) version 4 data (Huang et al. 2016).

The initialization method used for CLT and MOD is exactly the same, which is a simple three-dimensional nudging method (Kang et al. 2014). The ocean temperature and salinity derived from the European Center for Medium-Range Weather Forecast (ECMWF) ocean reanalysis and ocean heat content datasets (ORAS4, Balmaseda et al. 2013) were used as observations. The observed ocean data

were nudged into the ocean model at all vertical layers with a specific relaxation time-scale of 3 days. It is noted that prediction results are not sensitive to the specified relaxation time-scale. No nudging processes were applied to the atmosphere, land and sea ice model components.

The coupled model was integrated with the nudging process over a 22-year spin-up period (1958-1979). The entire retrospective prediction period lasts 30 years starting from January 1st 1980 to December 31st 2009. The targeted seasons are boreal summer and winter with a 1- month lead time. The boreal summer (winter) prediction starts from 1st May (1st November). Each prediction contains four ensemble members. The lagged-averaged forecast (LAF) are employed for providing different initial perturbations for the ensemble members. The initial conditions for the four ensemble members were produced by 1-day time lagged ensemble method during the nudging process from 27th to 30th April for the 1st May boreal summer prediction. An increase in the ensemble size with the LAF method does not contribute to the skill improvement of the prediction (e.g. Kang et al. 2014).

For simplicity, temporal correlation coefficient (TCC) is used to evaluate skills of the ensemble mean prediction. The TCC was obtained by calculating the correlation coefficients between the observed and predicted values of given

variables during the 30 years of period (1980-2009). We have conducted two hindcast experiments with the CTL and MOD. In addition to the rainfall prediction, we also evaluated the predicted large-scale dynamic structure of EASM, including mean climatology, annual cycle, and major modes of interannual variability, as well as monsoon-ENSO relationship and circulation-rainfall teleconnection.

3. Performances on predicted EASM rainfall

Figure 1 presents the prediction skills of boreal summer mean precipitation over EA for the 30-year period (1980-2009) derived from the CTL and MOD. Wang et al. (2009) showed that while the MME prediction has considerable prediction skill score (more than 0.5) over the WNP, the prediction skills over the EA land regions are very low (< 0.2), suggesting that many climate models have no meaningful prediction skills over the continental EA. The CTL prediction shows low skills (< 0.2) over the EA except over the Yangtze River Valley (YRV) and Korea. The TCCs averaged over the EA domain (100-140°E, 5-50°N) are merely 0.04. This is mainly attributed to the negative skill over the eastern China Sea, southeastern China, SCS and Philippine Sea. The MOD prediction, in contrast, shows useful TCC scores ranging from 0.3 to 0.7 over the Yew River Valley and Korean peninsula, southeastern China and southern Japan, as well as the Philippine Sea and part of the

SCS. It is difficult to predict land monsoon rainfall due to complicate land surface conditions and the atmosphere-land interaction processes. For land EA, the CTL shows very low skill with a TCC of 0.03 but the MOD simulates much higher prediction skill score with a TCC of 0.37. Comparison of the CTL and MOD confirms that the MOD improves seasonal prediction considerably over EA. However, low skills are found over the YRV, Taiwan and eastern SCS. The possible reasons for the deficiency will be discussed in the next section.

Figure 2 shows year-to-year variations of the rainfall prediction skills measured by the Pattern Correlation Coefficient (PCC) between the observed and predicted JJA precipitation anomalies over the EASM domain. The Nino3.4 index was also shown in the figure to compare with the prediction skills. The CTL shows large amplitude fluctuation from year to year with moderate PCC score (~0.3) in 1980, 1987 and 1994 and negative PCCs for 17 years. The 30-year averaged PCC score is negative (-0.06). In the MOD, during high skill years (1982, 1993, 1997, 2004, 2005 and 2006), the PCC scores reaches about 0.6. The lowest negative PCC occurred in 2007. We compared the PCC scores during the El-Nino developing and decaying years, respectively (Figure 3). The CTL has pretty lower or negative skill during El-Nino developing and decaying years. On the other hand, the MOD has higher or

Peer-reviewed version available at Atmosphere 2018, 9, 487; doi:10.3390/atmos9120487

moderate skill during most of the El-Nino developing and decaying years, suggesting that the improved prediction skill in the MOD may be related with ENSO simulation and its teleconnection with EASM. The details will be discussed in the section 4.3.

4. Evaluation of predicted climatology and major modes of variability

To find out the reasons for the useful skills and deficiencies of the models' predictions, we try to analyze and identify the key factors that may influence the EASM prediction. These factors include predicted climatological mean states, the major modes of interannual variability, predicted Pacific SST anomalies and ENSO-EASM teleconnection, as well as the predicted WPSH and associated rainfall anomalies.

4.1 Climatology

Lee et al. (2010) demonstrated that the skill for individual coupled models in predicting seasonal precipitation anomalies is positively correlated with its performances on prediction of the annual mean and annual cycle of precipitation. For this reason, we examine the JJA large-scale climatological circulations and precipitation from observation and the models (Fig. 4). In observation, low-level

Peer-reviewed version available at Atmosphere 2018, 9, 487; doi:10.3390/atmos9120487

southwest monsoonal flows prevail from Arabian Sea through India and south Asia to Southern China, while southeasterlies blow from the Philippine Sea across East China Sea to Japan. In the CTL, the southwesterlies from Arabian Sea are simulated well but strong westerlies erroneously extend into the Philippine Sea and the northward flow over eastern China is weaker than the observation. The MOD well produces southwesterlies from the Arabian Sea and the southeasterlies from the western Pacific; but the northward flow over eastern China remains weak. This may induce insufficient northward moisture transport and weak subtropical precipitation. Over EA, the observed major subtropical rainfall is seen over China, Japan, Korea and surrounding seas (Meiyu, Changma and Baiu), which are associated with the quasi-stationary EA subtropical front. Also, there are heavy rain belt over the tropical monsoon trough extending from India via northern SCS to the Philippine Sea. The CTL underproduces the heavy rain belt over India and substantially overproduces heavy rain from the Bay of Bengal to western Pacific; meanwhile, the major subtropical rainfall is weaker than the observation (Fig. 4b). The MOD improves considerably the observed patterns of the tropical rain belt except that the heavy rainfall over the eastern Bay of Bengal shifts equatorward. The magnitude of rainfall over subtropical region is increased but still weaker than observation (Fig. 4c). In sum, the CTL predicts excessive rainfall over the SCS and

Philippine Sea and excessively strong monsoon trough over the Philippine Sea, but the MOD largely overcomes this deficiency. Yet, the MOD still underestimates the southerly flow over the eastern China Sea and associated subtropical frontal rainfall.

It is well known that the strength and location of the WPSH and westerly jet are vitally important for the EA rainfall distribution and its seasonal migration (Zhou and Yu 2005, Zhou et al. 2009, Wang et al. 2013). The observed WPSH (outlined by the isopleth of 5870 m) is over the subtropical Pacific along with strong westerly jet being located along 40°N and tropical easterly jet around 10°N. In the CTL, the WPSH is weak and the westerly jet is stronger and broader than the observation. In the MOD, the horizontal pattern of the 500 hPa geopotential height is improved (Fig. 4c). The magnitude of WPSH is comparable with observation except its location is slightly shifted eastward. The observed westerly jet is well represented in the MOD although its magnitude is slightly greater than observation. The results here suggest that the MOD has a potential for better EASM prediction by improved large-scale climatology compared to the CTL.

For skillful prediction of EASM rainfall, it is of preeminent importance to accurately simulate the seasonal transition from the dry to rainy seasons and associated northward movement of the Meiyu-Baiu rain belt (Wang et al. 2017).

Peer-reviewed version available at Atmosphere 2018, 9, 487; doi:10.3390/atmos9120487

Figure 5 shows a latitude-time diagram of the observation and predicted pentad mean rainfall from the CTL and MOD, averaged between 110°E and 130°E. Before mid-May, there are two major observed rainfall belts: 1) zonal band over 15°S-5°N and 2) subtropical band over EA (20°N-35°N). The later reflects spring rainy season over southern China. In mid-late May, the two rainfall belts merge together near 10°-25°N over the SCS. Around mid-June, the rainfall belt originally located at South China continuously moves northward up to 40°N and remains there until August. The CTL predicts the transition of rainfall reasonably well, but tropical rain belt is overproduced while the summer subtropical rain is significantly weaker than the observation. A more severe problem is that the CTL failed to predict northward propagation of rain belt from 25°N to 40°N. On the other hand, the MOD prediction reproduces not only better tropical rainfall that was overproduced in the CTL, but also better East Asian subtropical monsoon rainfall over north of 20°N, although the northward migration of the subtropical rain belt remains insufficient during August. This improvement made in MOD is expected to have a positive influence on the rainfall anomaly prediction over the northern EA.

4.2 ENSO prediction and EASM-ENSO relationship

ENSO has been recognized as the dominant source of predictability of EASM, which strongly affects EASM during both the ENSO developing and decaying summers (Fu et al. 1980, Huang and Wu 1989; Wang et al. 2017). Reliable seasonal forecast should rely on realistic prediction of ENSO and the EA rainfall and circulation system associated with it.

Figure 6 displays TCC skill of the models for Nino 3.4 SST anomalies as a function of forecast lead time. The North American Multi-model ensemble (NMME; Kirtman et al. 2014) was also shown in the figure to compare with the prediction skills. The TCC score of the CTL is 0.80 for boreal summer (averaged over the lead time of 1-3 months) but drops to 0.6 at 6-month lead. The summer mean skill score is much lower than the NMME and it is similar with the skill of the lowest dynamic model in the NMME members. The TCC score of the MOD is 0.87 for boreal summer and reaches 0.72 for 6-month lead. The TCC score of the MOD almost the same as the NMME skill, suggesting that the MOD has considerably improved ENSO prediction skill.

It is well known that EASM responds to ENSO differently in the developing summer and decaying summer. To this end, we examine the observed and model predicted EASM-ENSO relationship during the El Nino developing summer and

Peer-reviewed version available at Atmosphere 2018, 9, 487; doi:10.3390/atmos9120487

decaying summer, separately. The El Nino developing summer includes 1982, 1986, 1987, 1991, 1994, 1997, 2002, 2004, 2006 and 2009. The El Nino decaying summers are 1983, 1988, 1992, 1995, 1998, 2003, 2005, and 2007. Fig. 7 shows composite EASM precipitation and circulation anomalies derived from observation and predicted by the CTL and MOD. During El Nino developing summer, the observed summer rainfall deceases over the central and northern EA but increases over the southern EA, in accordance with the cyclonic anomalies over the southern EA and the anticyclonic anomalies over the northern China. The CTL captures the dry anomalies over the Yellow Sea to west of Korea and Yangtze River Valley but failed to simulate the wet anomalies over the southern EA. Corresponding westerlies over the SCS and Philippine Sea is simulated in the CTL but anomalous easterlies shift to Korea. The anticyclonic anomalies over the northern China ae not simulated in the CTL. The MOD well captures dry anomalies over the central and northern EA and wet anomalies over the southern EA and WP as well as the cyclonic anomalies over southern EA and anticyclonic anomalies over northern China. However, the magnitudes of the circulation and rainfall anomalies are too strong. There is also a wet bias in the northern China.

Peer-reviewed version available at Atmosphere 2018, 9, 487; doi:10.3390/atmos9120487

During El Nino decaying summer, observation displays dry rainfall anomalies over the SCS and Philippine Sea and wet anomalies over Meiyu front, which correspond to an anticyclonic anomaly in the SCS and Philippine Sea. The CTL failed to capture both the dry anomalies over South EA (except over the Philippine Sea) and the wet anomalies over central China (Meiyu front) and Korea. The corresponding anticyclonic anomalies in the SCS and Philippine Sea is simulated in the CTL with a weak magnitude. The MOD simulates more realistic dry anomalies over the SCS and the wet anomalies north of 25°N but with strong dry biases over the northern East China. The anticyclonic anomalies in the MOD resemble the observed counterparts. Generally, the MOD well reproduces rainfall anomalies related with ENSO over the southern and northern EA, where its prediction skill tends to be higher than other regions. Similarly, the CTL has better rainfall anomalies around Korea, where the prediction skill is relatively high. The results suggest that a better EASM-ENSO relationship may contributes to the improvement of rainfall prediction skill.

4.3 Major modes of interannual variability of EASM

Besides climatology, it is important to see the model's capability in predicting intrinsic modes of interannual variability. We argue that models with better intrinsic

modes of interannual variability may improve EASM prediction. To depict the major modes of variability, Wang (1992) suggested multivariate EOF analysis (MV-EOF) by analyzing a set of meteorological and oceanographic fields. The leading MV-EOF mode can be a good indicator for estimating variability of EASM that has special structures in both precipitation and circulation systems.

Figure 8 (upper panels) shows the first MV-EOF mode of the JJA precipitation and 850hPa zonal winds anomalies from the observation and predicted by the models. The observation displays dry rainfall anomalies over the SCS and Philippine Sea and wet anomalies over Meiyu front region, which correspond to an anticyclonic anomaly in the SCS and Philippine Sea and a cyclonic anomaly located to the east of Korea with a relatively weak magnitude. The CTL captures dry anomalies over the Philippine Sea but there is strong wet bias over the southern SCS. The CTL also poorly produces the wet anomaly along the subtropical frontal zone from the southern to west Japan. The MOD has an overall similar performance and deficiencies as in the CTL. The WP anticyclonic anomalies are weak and the cyclonic anomaly northeast of Korea is missed in both the CTL and MOD. The rainfall anomalies over the subtropical EA, especially over the Yangtze River Valley are

totally missed, which is partially responsible for the low skills over the YRV in the MOD prediction.

The interannual variation of the corresponding principal component of the first mode is shown in Fig. 8d and e. The observed PCs generally have higher (lower) value at El-Nino decaying (developing) year. The PCs of CTL are weakly correlated with the observed PCs (CC: 0.28), while the PCs from the MOD and observation are significantly correlated but the CC (0.55) is not very high.

4.4 **Prediction of EASM circulation index and associated rainfall anomaly pattern**

Previous studies have shown that the models have better ability to predict the circulation anomalies over the WNP-EA region, although precipitation anomalies are poorly predicted (Fan et al. 2012). Here we examine whether this is the case for the CTL and MOD or not. The variation of the WNP-EASM circulation system is well depicted by the meridional zonal wind shear (vorticity) index defined by 850hPa zonal wind averaged over (22.5–32.5°N, 110–140°E) minus that over (5–15°N, 90–130°E) proposed by Wang and Fan (1999). This WF index captures variations of the WNP tropical monsoon trough, the WPSH and associated subtropical frontal

zone (Wang et al. 2008). The strength and location of the WPSH is one of dominant factor for EA rainfall (Zhou et al. 2009b; Wang et al. 2013) and it represents well the leading mode of EASM variations (Wang et al. 2008). Figure 9 shows prediction skill score for the WF index. The observation displays that positive (negative) WF index tends to be related with El-Nino decaying (developing) year. The CTL performs poorly in capturing the year-to-year variability with a temporal correlation coefficient (TCC) score of 0.20. The MOD simulates the interannual variability of WF index reasonably well with a TCC of 0.64. This is consistent with the improved MOD performance in predicting the EASM-ENSO relationship (Fig. 7).

The improved prediction for zonal wind can further enhance WPSH-rainfall relationship. Figure 10 shows regressed JJA rainfall and circulation anomalies on the WFI from observation and the models. Observation shows dry anomalies over the Philippine Sea and northern SCS and wet anomaly along EA subtropical front over the YRV, South Korea and Japan in association with enhanced WPSH. The CTL fails to capture wet anomalies over central and northern EA including Korea and Japan and dry anomalies over SCS. Overall, the CTL simulates rainfall anomalies poorly with a PCC of 0.57 and a normalized root mean square error (NRMSE) of 0.92. The MOD predicts better the pattern of rainfall anomalies with an increased PCC of 0.71

Peer-reviewed version available at Atmosphere 2018, 9, 487; doi:10.3390/atmos9120487

and a reduced NRMSE of 0.76. The results suggest that better prediction of the circulation index tends to reproduce better rainfall prediction, which is consistent with previous studies (Wang and Fan 1999; Zhang et al. 2003; Li et al. 2012).

5. Conclusion and discussion

This study assessed the seasonal prediction skill of the Nanjing University of Information Science and Technology Earth System Model (NESM3.0) for East Asia Summer Monsoon (EASM). The earlier version of NESM3.0 has poor performance in seasonal prediction of EASM. In order to improve the model prediction, the convective parameterization schemes are modified to suppress excessive deep convection and enhance insufficient shallow and stratiform clouds over the tropics (Section 2.2). The new version of NESM3.0 with modified parameterizations (MOD) yields markedly improved rainfall prediction in large areas of EA land regions except over the Yangtze River Valley (YRV) (Fig. 1). The diagnostic analysis based on large-scale dynamic structure were carried out to find key processes responsible for better prediction and remaining deficiencies. It is found that the improved prediction is primarily attributed to the improvements in the MOD predicted (i) climatological summer mean rainfall especially over the WP monsoon trough and the WP subtropical high (Fig. 4); (ii) the seasonal march of the subtropical rain belt

over EA (Fig. 5), the ENSO prediction (Fig. 6) and the EA rainfall anomalies associated with the development and decay of El Nino events (Fig. 7). However, the MOD still has notable biases in the predicted leading mode of interannual variability of precipitation. The leading mode captures the dry (wet) anomalies over the South China Sea (northern EA) but misplaced precipitation anomalies over the Yangtze River Valley and along the subtropical front in general (Fig. 8). The model can capture the interannual variation of the circulation indices very well (Fig. 9), but the bias in the circulation-rainfall connection caused predicted rainfall errors. The results here suggest that over EA land regions, the skillful rainfall prediction relies on not only model's capability in predicting better summer mean and seasonal march of rainfall and ENSO teleconnection with EASM, but also accurate prediction of the leading modes of interannual variability, especially the anomalous western Pacific subtropical high (WPSH) and its connections with the EA rainfall. The results here also suggest that the model with better dynamics structure may reproduce better prediction of precipitation over EA. This issue will be studied in the further study.

This study focused on large-scale dynamic structure to reveal which processes is critical to improved prediction. However, other physical processes (e.g.

thermodynamic, moisture, land surface feedback, etc.) may all contribute to prediction skill of rainfall over EA. These invite future studies. It would be worthwhile to estimate impacts of each large-scale dynamic features on improved prediction and clearly identify how they contributed to the improvements. But this requires a large set of multi-model ensemble hindcast data. This is another topic for future study. While we have assessed the impacts of the modified parameterizations as a whole on EASM prediction, explanation for how each modified parameterization affects seasonal prediction skill remains difficult. Since many modifications in the physical processes were employed in the model, additional experiments need to be conducted to identify the effects of each modification.

Although notable improvement has been made in the model, there remains large room for further improvement. Previous studies suggested that deficit of cloud physics or convective parameterization in the models results in low prediction skill (Lee et al., 2010; Seo et al., 2015). The introduction of stochastic parameters in the major physical processes (e.g. convective parameterization, cloud microphysics) can be one of solution to improve parameterization because it is difficult to find accurate parameter values. Also, adapting more advanced initialization methods (e.g.

Ensemble Kalman filter) may increase predictability. These will be the subjects of further study.

Acknowledgements

This work is supported by National Natural Science Foundation of China (Grant No. 41420104002) and the National Key Research and Development Program of China (Grant No. 2016YFA0600401) as well as the National Science Foundation (Climate Dynamics Division) Award No. AGS-1540783. This is Publication No. XXXX of the SOEST, Publication No. YYYY of IPRC, and Publication No. ZZ of the Earth System Modeling Center (ESMC).

Reference

Adler, R. F., and Coauthors, 2003: The Version-2 Global Precipitation Climatology Project (GPCP) Monthly Precipitation Analysis (1979–Present). *J Hydrometeorol*, 4, 1147-1167.

Cao, J.; Wang, B.; Yang, Y.-M.; Ma, L.; Li, J.; Sun, B.; Bao, Y.; He, J.; Zhou, X. The nuist earth system model (nesm) version 3: Description and preliminary evaluation. *Geosci. Model Dev. Discuss. (accepted)* 2018, *1*.

Chang, C. P., and K. M. Lau, 1982: Short-Term Planetary-Scale Interactions over the

Tropics and Midlatitudes during Northern Winter. Part I: Contrasts between Active and Inactive Periods. *Mon Weather Rev*, 110, 933-946.

Chang, C. P., 2004: *East Asian Monsoon*. World Scientific.

Chen, W., G. Hans-F, and R. Huang, 2000: The interannual variability of East Asian Winter Monsoon and its relation to the summer monsoon. *Adv Atmos Sci*, 17, 48-60.

Craig, A., S. Valcke, and L. Coquart, 2017: Development and performance of a new version of the OASIS coupler, OASIS3-MCT_3.0. *Geosci. Model Dev.*, 10, 3297-3308.

Dao, S.-Y., and L.-S. Chen, 1957: The Structure of General Circulation over Continent of Asia in Summer. *Journal of the Meteorological Society of Japan. Ser. II*, 35A, 215-229.

Fan, K., Y. Liu, and H. Chen, 2012: Improving the prediction of the East Asian summer monsoon: New approaches. *Wea. Forecasting*, 27, 1017–1030, doi:https://doi.org/10.1175/WAF-D-11-00092.1

Gong, H., L. Wang, W. Chen, R. Wu, K. Wei, and X. Cui, 2013: The Climatology and Interannual Variability of the East Asian Winter Monsoon in CMIP5 Models. *J Clim*, 27, 1659-1678.

Huang, B., and Coauthors, 2015: Further Exploring and Quantifying Uncertainties for Extended Reconstructed Sea Surface Temperature (ERSST) Version 4 (v4). *J Clim*, 29, 3119-3142.

Huang, R., and Y. Wu, 1989: The influence of ENSO on the summer climate change in China and its mechanism. *Adv Atmos Sci*, 6, 21-32.

Huang, R., J. Chen, and G. Huang, 2007: Characteristics and variations of the East Asian monsoon system and its impacts on climate disasters in China. *Adv*

Atmos Sci, 24, 993-1023.

Hunke, E. C., and W. H. Lipscomb, 2010: *CICE: The Los Alamos Sea Ice Model Documentation and Software User's Manual Version 4.1. LA-CC-06-012.* T-3 Fluid Dynamics Group.

Jhun, J.-G., and E.-J. Lee, 2004: A New East Asian Winter Monsoon Index and Associated Characteristics of the Winter Monsoon. *J Clim*, 17, 711-726.

Jiang, D., and Z. Tian, 2013: East Asian monsoon change for the 21st century: Results of CMIP3 and CMIP5 models. *Chinese Sci Bull*, 58, 1427-1435.

Kanamitsu, M., W. Ebisuzaki, J. Woollen, S.-K. Yang, J. J. Hnilo, M. Fiorino, and G. L. Potter, 2002: NCEP–DOE AMIP-II Reanalysis (R-2). *B Am Meteorol Soc*, 83, 1631-1643.

Kang, I. S., and Coauthors, 2002: Intercomparison of the climatological variations of Asian summer monsoon precipitation simulated by 10 GCMs. *Clim Dyn*, 19, 383-395.

Kang, I. S., and Co-authors, 2014: Examination of multi-perturbation methods for ensemble prediction of the MJO during boreal summer. *Clim Dyn*, 42, 2627–2637.

Lau, K.-M., and M.-T. Li, 1984: The Monsoon of East Asia and its Global Associations—A Survey. *B Am Meteorol Soc*, 65, 114-125.

Lee, D. Y. and co-authors, 2015: Enhancement of seasonal prediction of East Asian summer rainfall related to western tropical Pacific convection. *Clim. Dyn.* 45, 1025–1042.

Lee, J.-Y., and B. Wang, 2014: Future change of global monsoon in the CMIP5. *Clim Dyn*, 42, 101-119.

Lee, J.-Y., B. Wang and co-authors, 2010: How are seasonal prediction skills related

to models performance on mean state and annual cycle? *Climate Dyn.*, 35, 267-283, doi: 10.1007/s00382-010-0857-4.

Li, C. Y., 1990: Interaction between anomalous winter monsoon in East Asia and El Nino events. *Adv Atmos Sci*, 7, 36-46.

Li, Q., F. Wei, and D. Li, 2011: Interdecadal variation of East Asian summer monsoon and drought/flood distribution over eastern China in the last 159 years. *Journal of Geographical Sciences*, 21, 579-593.

Lu, R., and Y. Fu, 2009: Intensification of East Asian Summer Rainfall Interannual Variability in the Twenty-First Century Simulated by 12 CMIP3 Coupled Models. *J Clim*, 23, 3316-3331.

Madec, G., 2008: *NEMO ocean engine.* Note du Pole de modélisation, Institut Pierre-Simon Laplace (IPSL), NO 27, ISSN No 1288-1619.

Man, W., T. Zhou, and J. H. Jungclaus, 2012: Simulation of the East Asian Summer Monsoon during the Last Millennium with the MPI Earth System Model. *J Clim*, 25, 7852-7866.

Meehl, G. A., and Coauthors, 2007: THE WCRP CMIP3 Multimodel Dataset: A New Era in Climate Change Research. *B Am Meteorol Soc*, 88, 1383-1394.

Nordeng, T. E. (1994). Extended versions of the convective parametrization scheme at ECMWF and their impact on the mean and transient activity of the model in the tropics, European Centre for Medium-Range Weather Forecasts.

Rayner, N. A., and Coauthors, 2003: Global analyses of sea surface temperature, sea ice, and night marine air temperature since the late nineteenth century. *J Geophys Res*, 108, 4407.

Seo, K.-H., J. Ok, J.-H. Son, and D.-H. Cha, 2013: Assessing Future Changes in the East Asian Summer Monsoon Using CMIP5 Coupled Models. *J Clim*, 26,

7662-7675.

Song, F., and T. Zhou, 2013: Interannual Variability of East Asian Summer Monsoon Simulated by CMIP3 and CMIP5 AGCMs: Skill Dependence on Indian Ocean–Western Pacific Anticyclone Teleconnection. *J Clim*, 27, 1679-1697.

Sperber, K. R., and Coauthors, 2013: The Asian summer monsoon: an intercomparison of CMIP5 vs. CMIP3 simulations of the late 20th century. *Clim Dyn*, 41, 2711-2744.

Stevens, B., and Coauthors, 2017: The Atmospheric Component of the MPI-M Earth System Model: ECHAM6. *Journal of Advances in Modeling Earth Systems*.

Taylor, K. E., R. J. Stouffer, and G. A. Meehl, 2011: An Overview of CMIP5 and the Experiment Design. *B Am Meteorol Soc*, 93, 485-498.

Tiedtke, M. (1989). "A comprehensive mass flux scheme for cumulus parameterization in large-scale models." Monthly Weather Review 117(8): 1779-1800.

Tompkins, A. M., Ortiz De Zarate, M. I., Saurral, R. I., Vera, C., Saulo, C., Merryfield, W. J., Sigmond, M., Lee, W. S., Baehr, J., Braun, A., Butler, A., Deque, M., Doblas-Reyes, F. J., Gordon, M., Scaife, A. A., Imada, Y., Ishii, M., Ose, T., Kirtman, B., Ku- mar, A., Muller, W. A., Pirani, A., Stockdale, T., Rixen, M., and Yasuda, T.: The Climate-System Historical Forecast Project: Pro- viding Open Access to Seasonal Forecast Ensembles from Cen- ters around the Globe, B. Am. Meteorol. Soc., 98, 2293–2302, https://doi.org/10.1175/Bams-D-16-0209.1, 2017.

Wang, B., 1992: The vertical structure and development of the ENSO anomaly mode during 1979-1989. *J Atmos Sci*, 49, 698-712.

Wang, B., and Z. Fan, 1999: Choice of South Asian Summer Monsoon Indices. *B Am Meteorol Soc*, 80, 629-638.

Wang, B., Y. Zhang, and M. Lu, 2004: Definition of South China Sea Monsoon Onset and Commencement of the East Asia Summer Monsoon. *J Clim*, 17, 699-710.

Wang, B., Q. Ding, X. Fu, I.-S. Kang, K. Jin, J. Shukla, and F. Doblas-Reyes, 2005: Fundamental challenge in simulation and prediction of summer monsoon rainfall. *Geophys. Res. Lett.*, Vol. 32, No. 15, L15711, doi: 10.1029/2005GL022734 12.

Wang, B., 2006: *The Asian Monsoon.* Springer-Praxis.

Wang, B., Z. Wu, J. Li, J. Liu, C. P. Chang, Y. Ding, and G. Wu, 2008: How to measure the strength of the East Asian summer monsoon. *J Clim*, 21, 4449-4463.

Wang, B., Lee, J.-Y., Kang, I.-S., Shukla, J., Park, C. K., Kumar, A., Schemm, J., Cocke, S., Kug, J. S., Luo, J. J., Zhou, T., Wang, B., Fu, X., Yun, W. T., Alves, O., Jin, E. K., Kinter, J., Kirt- man, B., Krishnamurti, T., Lau, N. C., Lau, W., Liu, P., Pegion, P., Rosati, T., Schubert, S., Stern, W., Suarez, M., and Yam- agata, T.: Advance and prospectus of seasonal prediction: as- sessment of the APCC/CliPAS 14-model ensemble retrospective seasonal prediction (1980–2004), Clim. Dynam., 33, 93–117, https://doi.org/10.1007/s00382-008-0460-0, 2009.

Wang, B., Z. Wu, C. P. Chang, J. Liu, J. Li, and T. Zhou, 2010: Another look at interannual-to-interdecadal variations of the East Asian winter monsoon: The northern and southern temperature modes. *J Clim*, 23, 1495-1512.

Wang, B., B. Xiang, and J.-Y. Lee, 2013: Subtropical High predictability establishes a promising way for monsoon and tropical storm predictions. *Proc Natl Acad Sci*, 110, 2718-2722.

Wang, B., J. Li, and Q. He, 2017: Variable and robust East Asian monsoon rainfall response to El Niño over the past 60 years (1957–2016). *Adv Atmos Sci*, 34, 1235-1248.

Wang, L., R. Huang, L. Gu, W. Chen, and L. Kang, 2009b: Interdecadal Variations of the East Asian Winter Monsoon and Their Association with Quasi-Stationary Planetary Wave Activity. *J Clim*, 22, 4860-4872.

Webster, P. J., V. O. Magaña, T. N. Palmer, J. Shukla, R. A. Tomas, M. Yanai, and T. Yasunari, 1998: Monsoons: Processes, predictability, and the prospects for prediction. *J. Geophys. Res.*, 103, 14451-14510.

Wei, K., T. Xu, Z. Du, H. Gong, and B. Xie, 2014: How well do the current state-of-the-art CMIP5 models characterise the climatology of the East Asian winter monsoon? *Clim Dyn*, 43, 1241-1255.

Wen, M., S. Yang, A. Kumar, and P. Zhang, 2009: An Analysis of the Large-Scale Climate Anomalies Associated with the Snowstorms Affecting China in January 2008. *Mon Weather Rev*, 137, 1111-1131.

Wen, L., K. Zhao, G. Zhang, B. Zhou, S. Liu, X. Chen, and M. Xue, 2016: Statistical characteristics of raindrop size distributions observed in east China during the Asian summer monsoon season from the 2D-video disdrometer and micro-rain radar. *J. Geophy. Res.*, 121, 2265–2282.

Yang, Y-M. and B. Wang, 2018: Improving MJO simulation by enhancing the interaction between boundary layer convergence and lower tropospheric heating, *Clim Dyn*, *Accepted*.

Yang, S. & Smith, E. A. Convective-stratiform precipitation variability at seasonal scale from 8 yr of trmm observations: implications for multiple modes of diurnal variability. *J. Clim.* 21, 4087–4114 (2008) .

Yang, S., Zhang, Z. Q., Kousky, V. E., Higgins, R. W., Yoo, S. H., Liang, J. Y., and Fan, Y.: Simulations and seasonal prediction of the Asian summer monsoon in the NCEP Climate Forecast System, J. Climate, 21, 3755–3775, https://doi.org/10.1175/2008jcli1961.1, 2008.

Xie, P., and P. A. Arkin, 1997: Global Precipitation: A 17-Year Monthly Analysis Based on Gauge Observations, Satellite Estimates, and Numerical Model Outputs. *B Am Meteorol Soc*, 78, 2539-2558.

Zhang, Y., K. R. Sperber, and J. S. Boyle, 1997: Climatology and Interannual Variation of the East Asian Winter Monsoon: Results from the 1979–95 NCEP/NCAR Reanalysis. *Mon Weather Rev*, 125, 2605-2619.

Zhou, T., and Z. Li, 2002: Simulation of the east asian summer monsoon using a variable resolution atmospheric GCM. *Clim Dyn*, 19, 167-180.

Zhou, T., and Coauthors, 2009a: Why the Western Pacific Subtropical High Has Extended Westward since the Late 1970s. *J Clim*, 22, 2199-2215.

Zhou, T.-J., and R.-C. Yu, 2005: Atmospheric water vapor transport associated with typical anomalous summer rainfall patterns in China. *J Geophys Res: Atmos*, 110, n/a-n/a.

Zhou, W., J. C. L. Chan, W. Chen, J. Ling, J. G. Pinto, and Y. Shao, 2009b: Synoptic-

Scale Controls of Persistent Low Temperature and Icy Weather over Southern China in January 2008. *Mon Weather Rev*, 137, 3978-3991.

Zhu, Z., J. He, and L. Qi, 2012: Seasonal transition of East Asian subtropical monsoon and its possible mechanism. *J Trop Meteorol*, 18, 305-311.

Zhu, Z., T. Li, and J. He, 2014: Out-of-Phase Relationship between Boreal Spring and Summer Decadal Rainfall Changes in Southern China. *J Clim*, 27, 1083-1099.

Zhu, Z., and T. Li, 2017: Empirical prediction of the onset dates of South China Sea summer monsoon. *Clim Dyn*, 48, 1633-1645.

Figure captions

FIG.1 Temporal correlation coefficient of JJA mean precipitation from (a) CTL and (b) MOD over EA during 1980-2009. The green and black contour represent a coefficient of 0.5 and 0.3, respectively.

FIG. 2 Year-to-year variations of the precipitation prediction skill (red line) measured by PCC between observation and predicted JJA rainfall from (a) CTL and (b) MOD during 1980-2009. PCCs were calculated over the EASM domain (5-40ºN, 100-140ºE). The blue bars represent observed DJF Nino3.4 SST Index

FIG. 3 Same as Fig. 2 except for El-Nino (a) developing and b) decaying years.

Fig.4 JJA large-scale climatology from (a) observation, (b) CTL and (c) MOD. Left panels represent precipitation (shading, mm/day), geopotential height (contours, m) and winds (vectors, m/s) at 850hPa. Right panels show zonal wind at 200 hPa (shading, m/s) and 500-hPa geopotential height (contours, m).

FIG. 5 Annual cycle climatology (1980-2009) for pentad mean precipitation averaged between 110˚E and 130˚E from (a) observation, (b) CTL and (c) MOD. The blue horizontal line shows 20°N.

FIG. 6 TCC skill of the JJA Nino 3.4 SST index from CTL (blue), MOD(red), NMME (black) and lowest dynamic models (gray dashed) from NMME project as a function of lead month. The forecast starts from May 1st.

Fig. 7 Composite maps of JJA rainfall (shading) and 850 hPa winds (vector) anomalies from (a) observation (b) CTL and (c) MOD during El-Nino developing (upper panels) and decaying year (lower panels).

Fig. 8 Spatial patterns of first MV-EOF modes of JJA mean precipitation (shadings) and 850-hPa zonal wind (contour) from (a) observation, (b) CTL and (c) MOD during 30 years (1980-2009). Lower panels represent corresponding principal components from (d) CTL and (e) MOD.

Fig. 9 Year-to-year variations of the WF index from (a) CTL and (b) MOD. The WF index is defined by zonal wind at 850hPa over (22.5–32.5ºN, 110–140ºE) minus (5–15N, 90–130E). The black line represents observed WF.

Fig. 10 Regressed JJA wind (arrow), geopotential height (red contour) at 850hPa and precipitation (Shading) with respect to the WF index (defined in Fig.9) from (a) observation, (b) CTL and (c) MOD.

Figures

Preprints (www.preprints.org) | NOT PEER-REVIEWED | Posted: 29 August 2018 doi:10.20944/preprints201808.0500.v1

Peer-reviewed version available at Atmosphere 2018, 9, 487; doi:10.3390/atmos9120487

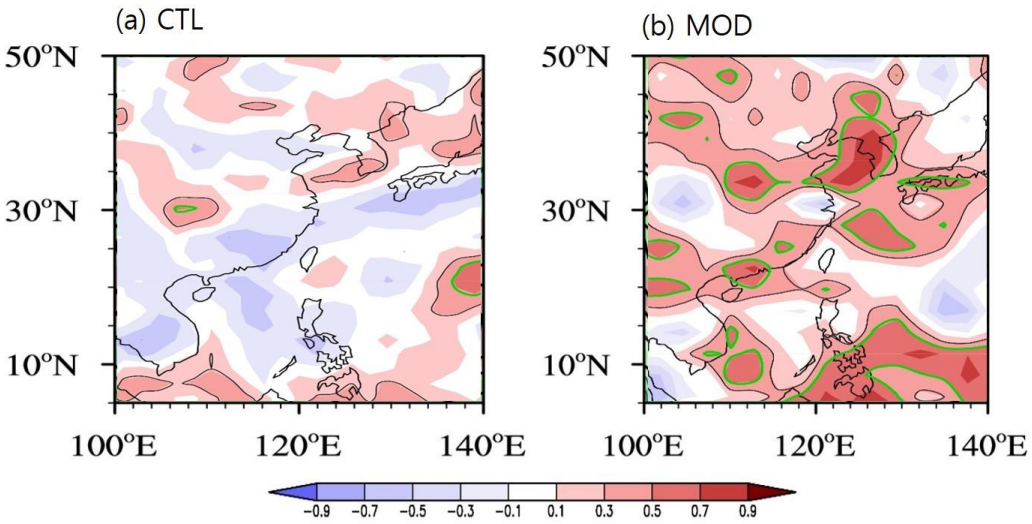

FIG.1 Temporal correlation coefficient of JJA mean precipitation from (a) CTL and (b) MOD over EA during 1980-2009. The green and black contour represent a coefficient of 0.5 and 0.3, respectively.

Preprints (www.preprints.org) | NOT PEER-REVIEWED | Posted: 29 August 2018 doi:10.20944/preprints201808.0500.v1

Peer-reviewed version available at Atmosphere 2018, 9, 487; doi:10.3390/atmos9120487

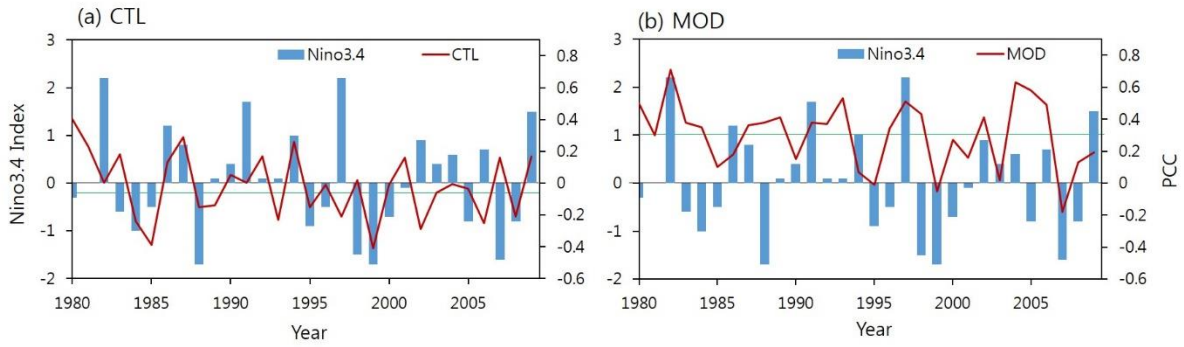

FIG. 2 Year-to-year variations of the precipitation prediction skill (red line) measured by PCC between observation and predicted JJA rainfall from (a) CTL and (b) MOD during 1980-2009. PCCs were calculated over the EASM domain (5-40ºN, 100-140ºE). The blue bars represent observed DJF Nino3.4 SST Index

Preprints (www.preprints.org) | NOT PEER-REVIEWED | Posted: 29 August 2018 doi:10.20944/preprints201808.0500.v1

Peer-reviewed version available at Atmosphere 2018, 9, 487; doi:10.3390/atmos9120487

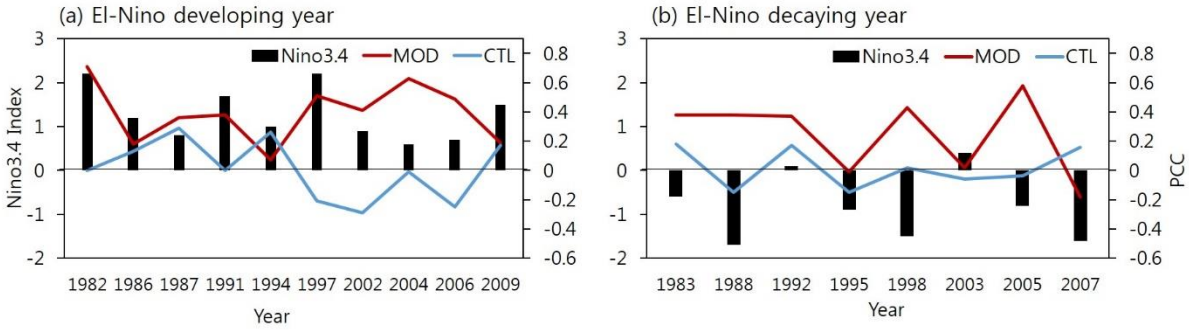

FIG. 3 Same as Fig. 2 except for El-Nino (a) developing and b) decaying years.

Preprints (www.preprints.org) | NOT PEER-REVIEWED | Posted: 29 August 2018 doi:10.20944/preprints201808.0500.v1

Peer-reviewed version available at Atmosphere 2018, 9, 487; doi:10.3390/atmos9120487

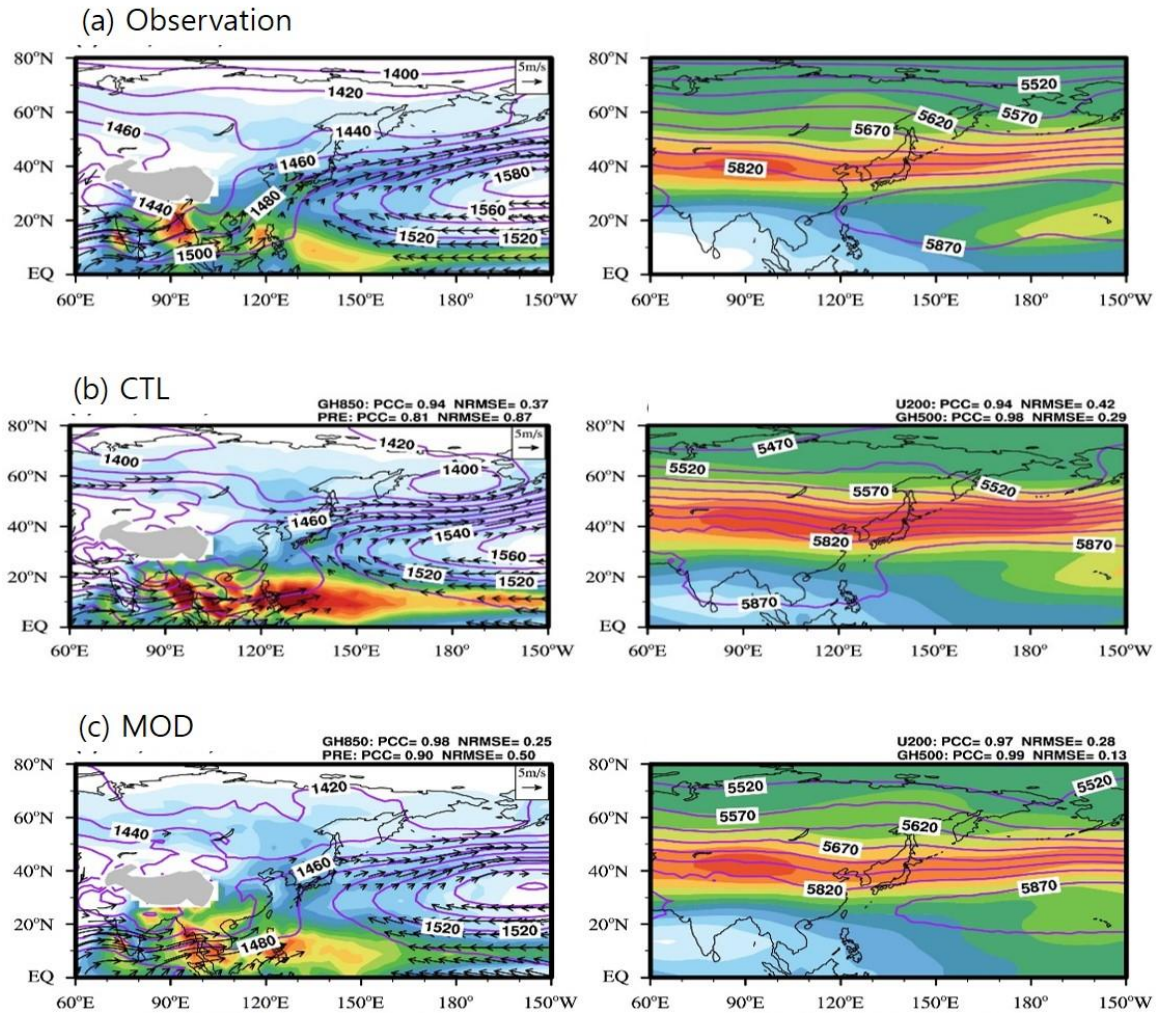

Fig.4 JJA large-scale climatology from (a) observation, (b) CTL and (c) MOD. Left panels represent precipitation (shading, mm/day), geopotential height (contours, m) and winds (vectors, m/s) at 850hPa. Right panels show zonal wind at 200 hPa (shading, m/s) and 500-hPa geopotential height (contours, m).

Preprints (www.preprints.org) | NOT PEER-REVIEWED | Posted: 29 August 2018 doi:10.20944/preprints201808.0500.v1

Peer-reviewed version available at Atmosphere 2018, 9, 487; doi:10.3390/atmos9120487

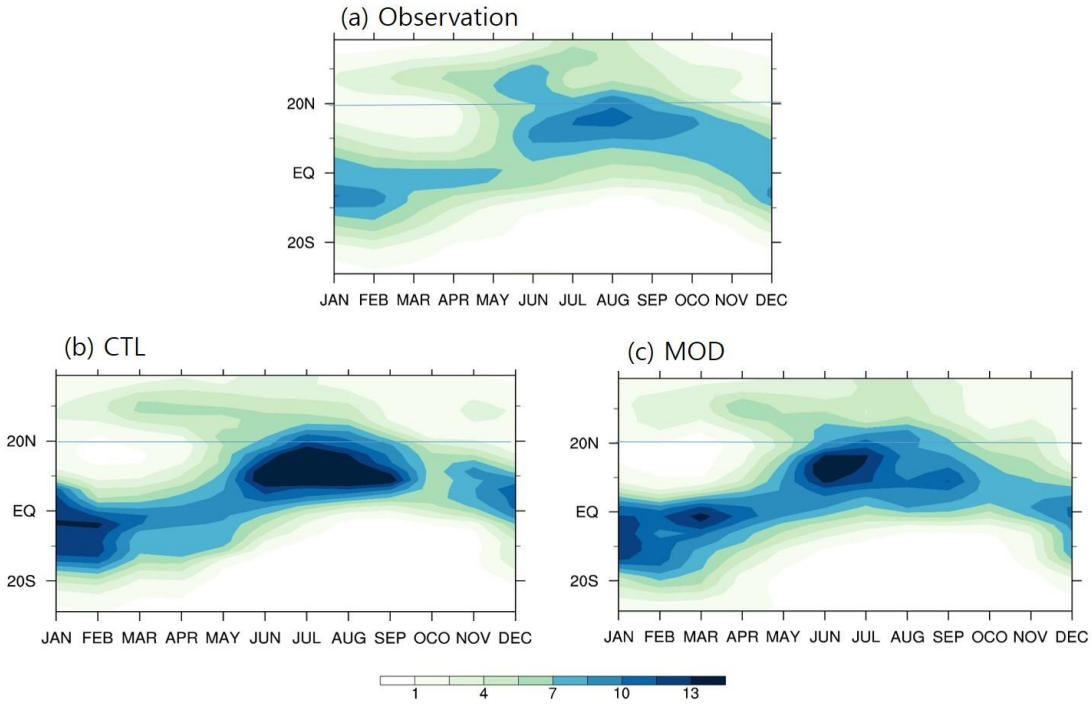

FIG. 5 Annual cycle climatology (1980-2009) for pentad mean precipitation averaged between 110˚E and 130˚E from (a) observation, (b) CTL and (c) MOD. The blue horizontal line shows 20°N.

Preprints (www.preprints.org) | NOT PEER-REVIEWED | Posted: 29 August 2018 doi:10.20944/preprints201808.0500.v1

Peer-reviewed version available at Atmosphere 2018, 9, 487; doi:10.3390/atmos9120487

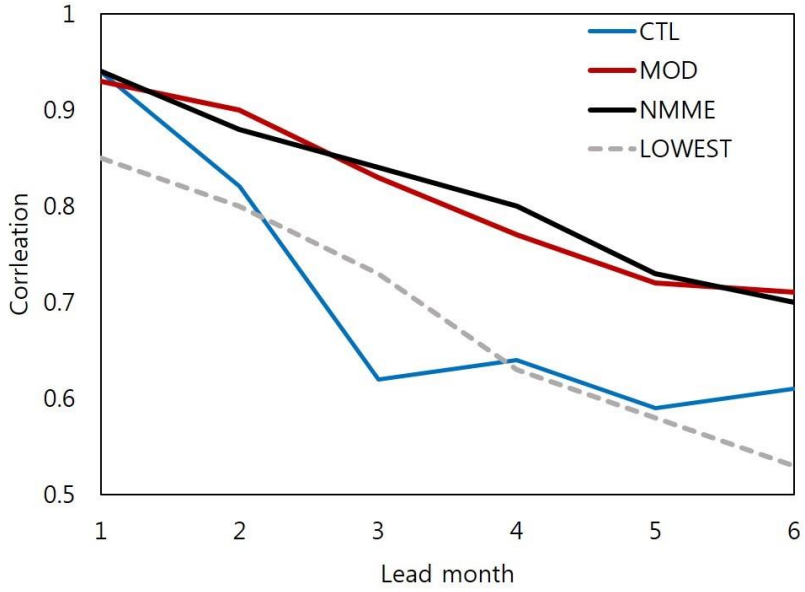

FIG. 6 TCC skill of the JJA Nino 3.4 SST index from CTL (blue), MOD(red), NMME (black) and lowest dynamic models (gray dashed) from NMME project as a function of lead month. The forecast starts from May 1st.

Preprints (www.preprints.org) | NOT PEER-REVIEWED | Posted: 29 August 2018 doi:10.20944/preprints201808.0500.v1

Peer-reviewed version available at Atmosphere 2018, 9, 487; doi:10.3390/atmos9120487

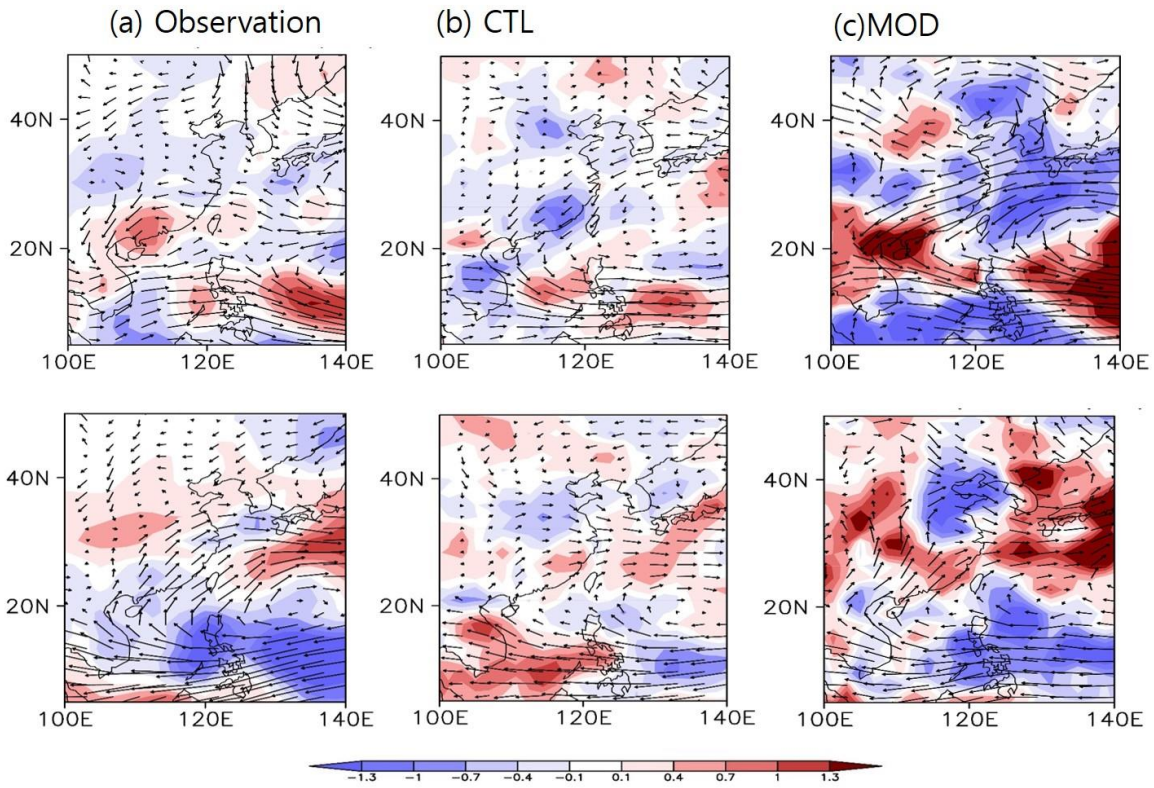

Fig. 7 Composite maps of JJA rainfall (shading) and 850 hPa winds (vector) anomalies from (a) observation (b) CTL and (c) MOD during El-Nino developing (upper panels) and decaying year (lower panels).

Preprints (www.preprints.org) | NOT PEER-REVIEWED | Posted: 29 August 2018 doi:10.20944/preprints201808.0500.v1

Peer-reviewed version available at Atmosphere 2018, 9, 487; doi:10.3390/atmos9120487

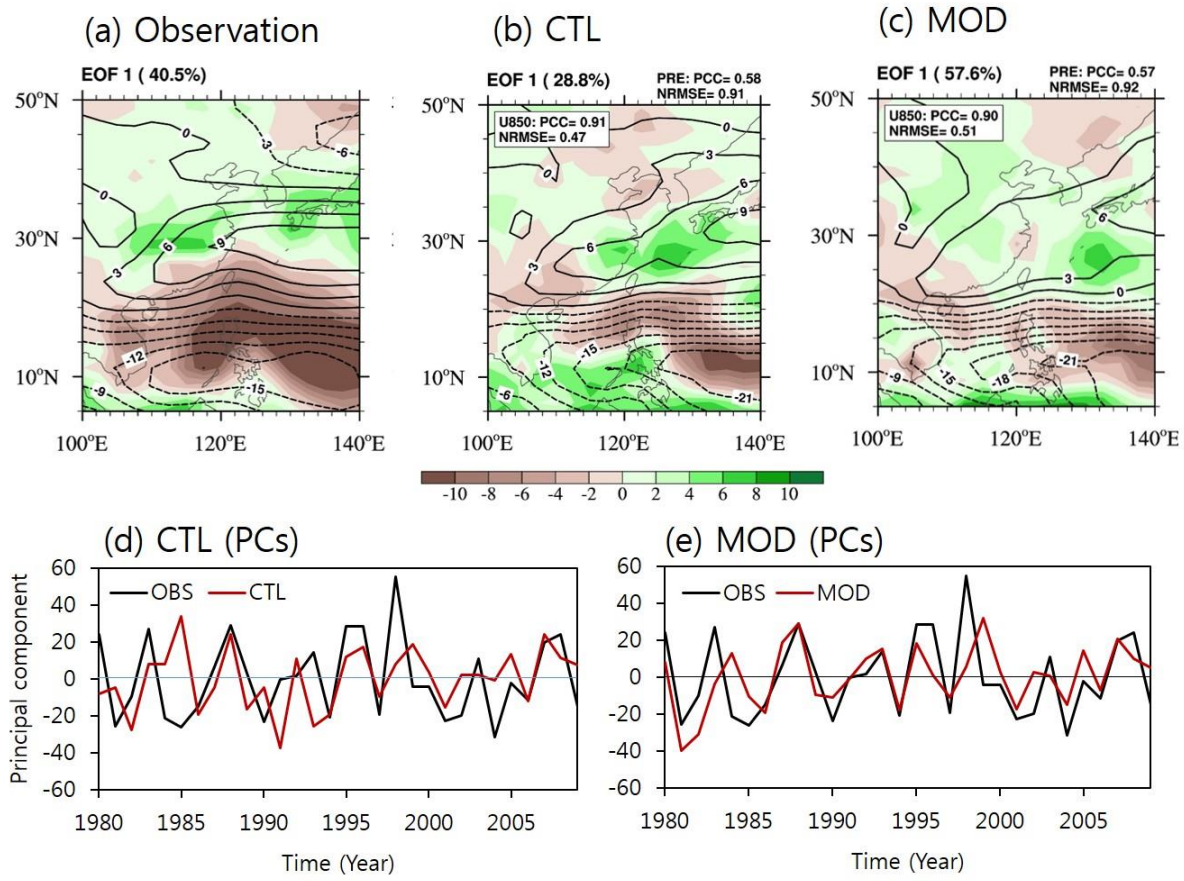

Fig. 8 Spatial patterns of first MV-EOF modes of JJA mean precipitation (shadings) and 850-hPa zonal wind (contour) from (a) observation, (b) CTL and (c) MOD during 30 years (1980-2009). Lower panels represent corresponding principal components from (d) CTL and (e) MOD.

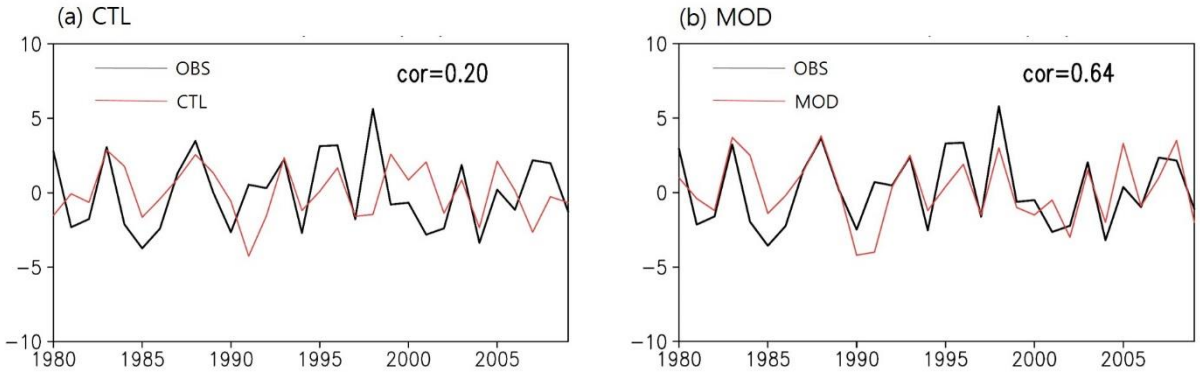

Fig. 9 Year-to-year variations of the WF index from (a) CTL and (b) MOD. The WF index is defined by zonal wind at 850hPa over (22.5–32.5ºN, 110–140ºE) minus (5–15N, 90–130E). The black line represnet observed WF.

Preprints (www.preprints.org) | NOT PEER-REVIEWED | Posted: 29 August 2018 doi:10.20944/preprints201808.0500.v1

Peer-reviewed version available at Atmosphere 2018, 9, 487; doi:10.3390/atmos9120487

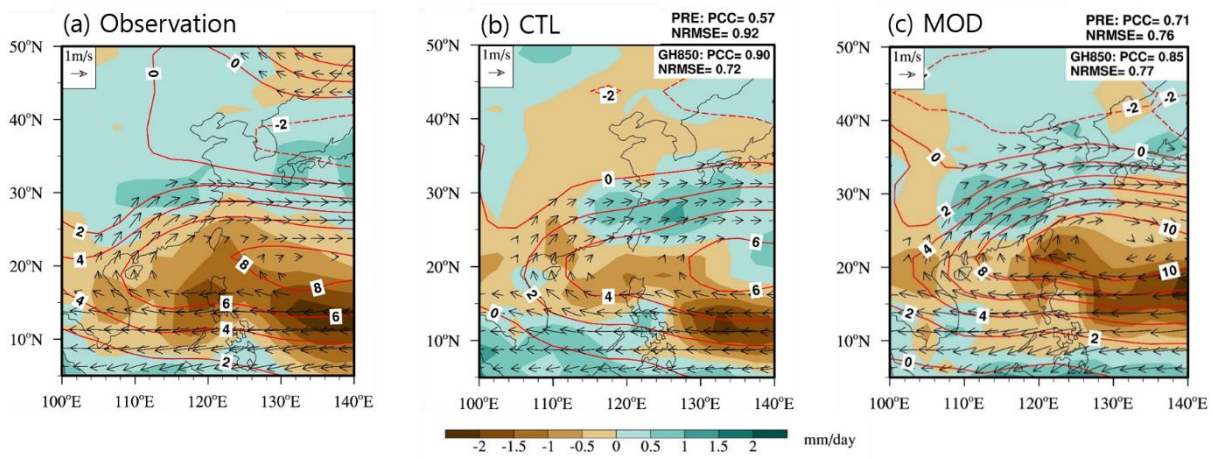

Fig. 10 Regressed JJA wind (arrow), geopotential height (red contour) at 850hPa and precipitation (Shading) with respect to the WF index (defined in Fig.9) from (a) observation, (b) CTL and (c) MOD.